

Article

Zinc Complexes of Fluorosubstituted *N*-[2-(Phenyliminomethyl)phenyl]-4-methylbenzenesulfamides: Synthesis, Structure, Luminescent Properties, and Biological Activity

Anatolii S. Burlov ¹, Valery G. Vlasenko ², Maxim S. Milutka ¹, Yurii V. Koshchienko ¹, Vladimir A. Lazarenko ³, Alexander L. Trigub ³, Alexandra A. Kolodina ¹, Alexander A. Zubenko ⁴, Elena V. Braga ⁵, Alexey N. Gusev ^{5,*} and Wolfgang Linert ⁶

¹ Institute of Physical and Organic Chemistry, Southern Federal University, 344090 Rostov-on-Don, Russia; anatoly.burlov@yandex.ru (A.S.B.); milutka@sfedu.ru (M.S.M.); yukoshch@ipoc.sfedu.ru (Y.V.K.); akolodina@sfedu.ru (A.A.K.)

² Institute of Physics, Southern Federal University, 344090 Rostov-on-Don, Russia; v_vlasenko@rambler.ru

³ National Research Centre “Kurchatov Institute”, 123182 Moscow, Russia; lazarenko_va@nrcki.ru (V.A.L.); alexander.trigub@gmail.com (A.L.T.)

⁴ North-Caucasian Zonal Scientific Research Veterinary Institute, Branch of the Federal State Budget Scientific Institution “Federal Rostov Agricultural Research Centre”, 344006 Rostov-on-Don, Russia; alexsandrzubenko@yandex.ru

⁵ General Chemistry Department, Crimean Federal University V.I. Vernadsky, 295007 Simferopol, Russia; braga.yelena@ya.ru

⁶ Institute of Applied Physics, Vienna University of Technology, Wiedner Hauptstraße 8-10, 1040 Vienna, Austria; wolfgang.linert@tuwien.ac.at

* Correspondence: galex0330@gmail.com



Citation: Burlov, A.S.; Vlasenko, V.G.; Milutka, M.S.; Koshchienko, Y.V.; Lazarenko, V.A.; Trigub, A.L.; Kolodina, A.A.; Zubenko, A.A.; Braga, E.V.; Gusev, A.N.; et al. Zinc Complexes of Fluorosubstituted *N*-[2-(Phenyliminomethyl)phenyl]-4-methylbenzenesulfamides: Synthesis, Structure, Luminescent Properties, and Biological Activity. *Materials* **2024**, *17*, 438. <https://doi.org/10.3390/ma17020438>

Abstract: Mono-, di-, and trifluorophenyl substituted in different positions of amine fragments bis [2-[[[(E)-(fluorophenyl)iminomethyl]-*N*-(*p*-tolylsulfonyl)anilino]zinc(II) complexes were synthesized. Their crystal structure, photo- and electroluminescent properties, and protistocidal, fungistatic, and antibacterial activities were studied. It has been shown that the introduction of fluorine atoms and an increase in their number in the ligand structure of the resulting metal complexes promote the luminescence quantum yields and values of performance and brightness in EL cells compared to their previously studied chlorine-substituted analogs.

Keywords: azomethines; zinc(II) complexes; photoluminescence; electroluminescence; biological activity

Academic Editor: Heesun Yang

Received: 6 December 2023

Revised: 27 December 2023

Accepted: 31 December 2023

Published: 17 January 2024



Copyright: © 2024 by the authors. Licensee MDPI, Basel, Switzerland. This article is an open access article distributed under the terms and conditions of the Creative Commons Attribution (CC BY) license (<https://creativecommons.org/licenses/by/4.0/>).

1. Introduction

The high demand for electroluminescent materials emitting in the range of 400–450 nm, i.e., blue emitters, is due to the fact that they are the main components of red–green–blue full-color displays and key electroluminescent components in the creation of white emitted by a blue and orange color combination [1]. Despite the fact that the number of luminophores emitting in the blue region is not inferior to the green and red phosphors, they significantly lose them in terms of stability in OLED (organic phosphors) and cost (iridium and osmium complexes). Therefore, the synthesis of new low-cost coordination compounds showing stable photoluminescence and electroluminescence in the blue region of the spectrum is still an important and urgent task.

The introduction of halogen atoms into ligand molecules, as previously shown, leads to an increase in the solubility and quantum yields (QY) of the photoluminescence (PL) and electroluminescence (EL) of their lanthanide(III) complexes [2–6]. A similar trend is characteristic of zinc(II) complexes based on the azomethine ligands 2-hydroxy- and

2-(*N*-tosylamino)benzaldehydes. The replacement of one or more C-H bonds by C-Cl and C-F bonds in the amine or aldehyde moieties of azomethines also leads to an increase in the PL QYs of the coordination compounds due to the quenching of vibrations [7–9]. The installation of the electron-withdrawing fluorine atoms helps to stabilize HOMO to widen the energy gap of the materials, thus realizing the blue emitter. It was found that zinc complexes with halogen-substituted azomethine ligands had photoluminescence quantum yields 2–4 times higher compared to unsubstituted ligands, both in solutions and in the solid state [10,11].

It has also been shown that, in azomethine metal complexes, the solubility and luminescence QYs increase significantly when the atomic number of the halogen substituent decreases and/or their number in the ligand increases. In this regard, the greatest effect is observed for fluorosubstituted azomethines and their metal complexes. In continuation of works on synthesis and the overall studies of PL and EL properties of the azomethine compounds of 2-hydroxybenzaldehydes and 2-*N*-tosylaminobenzaldehydes, here, we report the synthesis and comparative structural and photophysical studies of zinc complexes with fluoro-substituted azomethines and evaluate the impact of fluorine atoms' position on their luminescent properties. We have also performed some preliminary studies by using them as emitters for the fabrication of electroluminescent devices.

2. Materials and Methods

Commercially available starting materials (Alfa Aesar, Ward Hill, MA, USA) were used as purchased: Zinc acetate dihydrate (CAS# 5970-45-6), 2-fluoroaniline (CAS# 348-54-9), 4-fluoroaniline (CAS# 371-40-4), 3,4-difluoroaniline (CAS# 3863-11-4), 2, 4-difluoroaniline (CAS No. 367-25-9), 2,5-difluoroaniline (CAS No. 367-30-6), 2,6-difluoroaniline (CAS No. 5509-65-9), 3,5-difluoroaniline (CAS No. 372-39-4), and 2,4,6-trifluoroaniline (CAS No. 363-81-5).

The C, H, and N elemental analyses were carried out on a «EuroEA-3000» (EuroVector, Milan, Italy) analyzer. The amount of the metal was determined by the gravimetric method. The IR spectra of the obtained complexes were recorded on a Varian 3100-FTIR (Varian, Australia) Excalibur instrument in the range 4000–400 cm⁻¹ by the method of disturbed total internal reflection. The ¹H NMR spectra were obtained on a Varian Unity-300 (Varian, Australia) instrument (300 MHz) in DMSO-*d*₆.

The X-ray Zn K absorption edges of zinc complexes were obtained in the transmission mode at the Structural Materials Science station at the Kurchatov Synchrotron Center (Moscow, Russia) by the protocol described yearly [12]. The exact values of the nearest environment parameters of the zinc were determined by the IFFEFIT software package (version 1.2.11) [13,14]. More detailed information about the X-ray absorption experiment and EXAFS analysis can be found in the Supplementary Materials.

For the single crystals of the free ligands **1d**, **1f**, and zinc(II) complexes **2d**, **2h**, and **2f**, X-ray diffraction data were collected at the 'Belok' beamline of the Kurchatov Synchrotron Radiation Source (NRC Kurchatov Institute, Moscow, Russia) [15]. All data were collected at 100 K. The data were indexed and integrated by the XDS and XSCALE software suites (version 30 June 2023) [16]. The structures were solved by direct methods (intrinsic phasing) with SHELXT [17]. The structural models were investigated by Olex2 software (Olex2-1.5) [18] and refined by SHELXL [19] by a full-matrix least-squares method on F² with anisotropic displacements for all non-hydrogen atoms. Hydrogen atoms involved in H-bonding were refined isotropically. H-bonding-silent hydrogen atoms were placed into calculated positions and refined within the riding model with fixed isotropic displacement parameters.

The crystallographic parameters and the refinement statistics for **1d**, **1f**, **2d**, **2h**, and **2f** are given in Tables S1 and S2 (Supplementary Materials). Crystallographic data for these compounds have been deposited with the Cambridge Crystallographic Data Center, CCDC 2299391 (**1d**), 2299392 (**1f**), 2299394 (**2d**), 2299393 (**2h**), and 2299397 (**2f**), and can be obtained

free of charge from the Cambridge Crystallographic Data Centre via www.ccdc.cam.ac.uk/data_request/cif (accessed on 12 December 2023).

The luminescence of complexes and azomethines was carried out for both solutions and solid samples. The spectra were recorded on a FluoroMax-4 spectrofluorimeter (HORIBA Scientific, Kyoto, Japan). Quantum yields of emission were determined by the absolute method using an integrating sphere. Lifetime measurements were performed on a Horiba Fluorocube instrument (HORIBA Scientific, Kyoto, Japan) by time-correlated single-photon counting using a 365 nm LED excitation source.

Fabrication of the OLED was performed according to the methodology described earlier [10]: using “AUTO 306” equipment by “BOC EDWARDS” (Crawley, UK) for the thermal deposition of layers of sand quartz and detector SQM 160 (INFICON GmbH, New York, NY, USA) for the control of evaporation speed and the thickness of the deposited layers.

The voltage-current and luminance measurements of the obtained OLED structures were studied on a measuring complex consisting of a voltage analyzer source (Keithley 237, KEITHLEY, Cleveland, OH, USA) and a fiber spectrometer (AvaSpec-ULS-2048 × 64, Avantes BV, Apeldoorn, The Netherlands).

A detailed description of the methodology for studying the biological activity of new substances is given in our own previous works [20,21] and the Supplementary Materials.

2.1. General Procedure for the Synthesis of Azomethines **1a–h**

A solution of 5 mmol of fluorosubstituted aniline in 3 mL of glacial acetic acid was added to a solution of 1.38 g (5 mmol) 2-(*N*-tosylamino)benzaldehyde [22] in 3 mL of glacial acetic acid; then, the reaction mixture was refluxed for 2 h after cooling to r. t. Six mL of EtOH were added. The precipitate was filtered off, recrystallized from acetic acid, and dried in a vacuum tube at 100 °C.

N-[2-[(*E*)-(2-Fluorophenyl)iminomethyl]phenyl]-4-methyl-benzenesulfonamide (**1a**) was prepared from 1.38 g (5 mmol) of 2-(*N*-tosylamino)benzaldehyde and 0.56 g (5 mmol) 2-fluoroaniline. Yield 1.60 g (87%), orange powder, m.p. 133–134 °C (AcOH). IR spectrum (vas. oil), ν , cm^{-1} : 3285 (NH), 1624 s (CH=N), 1599, 1574, 1488, 1456, 1416, 1377, 1342 s (as SO₂), 1308, 1288, 1248, 1161 s (s SO₂), 1120, 1091, 1047, 971, 946, 879, 840, 814, 798, 759, 661, 619, 560. ¹H NMR (300 MHz, DMSO-*d*₆) δ : 2.28 (s, 3H, CH₃), 7.20 (tt, 1H, 3J = 7.4 Hz, 4J = 1.2 Hz, CAr-H), 7.30–7.38 (m, 5H, CAr-H), 7.43–7.53 (m, 3H, CAr-H), 7.68 (d, 2H, 3J = 8.1 Hz, CAr-H), 7.76 (dd, 1H, 3J = 7.8 Hz, 4J = 1.2 Hz, CAr-H), 8.83 (s, 1H, CH=N), 12.46 (s, 1H, NH). Found, %: C 65.24; N 4.71; S 7.65. C₂₀H₁₇FN₂O₂S. Calculated, %: C 65.20; N 4.65; S 7.60.

N-[2-[(*E*)-(4-Fluorophenyl)iminomethyl]phenyl]-4-methyl-benzenesulfonamide (**1b**) was prepared from 1.38 g (5 mmol) of 2-(*N*-tosylamino)benzaldehyde and 0.56 g (5 mmol) 4-fluoroaniline. Yield 1.55 g (85%), orange powder, m.p. 146–147 °C (AcOH). IR spectrum (vas. oil), ν , cm^{-1} : 3287, 3210 (NH), 1621 s (CH=N), 1596, 1573, 1497, 1463, 1455, 1427, 1402, 1378, 1338 s (as SO₂), 1309, 1292, 1243, 1228, 1167 s (s SO₂), 1155, 1117, 1090, 1047, 1019, 950, 884, 853, 833, 799, 776, 751, 728, 707, 662, 637, 616, 592, 568. ¹H NMR (300 MHz, DMSO-*d*₆) δ : 2.28 (s, 3H, CH₃), 7.17–7.22 (m, 1H, CAr-H), 7.29–7.41 (m, 6H, CAr-H), 7.44 (d, 2H, 4J = 3.6 Hz, CAr-H), 7.67 (d, 2H, 3J = 8.4 Hz, CAr-H), 7.74 (d, 1H, 3J = 7.5 Hz, CAr-H), 8.74 (s, 1H, CH=N), 12.43 (s, 1H, NH). Found, %: C 65.10; N 4.75; S 7.54. C₂₀H₁₇FN₂O₂S. Calculated, %: C 65.20; N 4.65; S 7.60.

N-[2-[[*E*)-(2,4-Difluorophenyl)iminomethyl]phenyl]phenyl]-4-methyl-benzenesulfonamide (**1c**) was prepared from 1.38 g (5 mmol) of 2-(*N*-tosylamino)benzaldehyde and 0.65 g (5 mmol) 2,4-difluoroaniline. The yield is 1.69 g (88%), an orange powder, m.p. 176–177 °C (AcOH). IR spectrum (vas. oil), ν , cm^{-1} : 3057 (NH), 1626 s (CH=N), 1597, 1574, 1540, 1495, 1463, 1403, 1377, 1339 s (as SO₂), 1291, 1267, 1229, 1168 s (s SO₂), 1156, 1142, 1116, 1092, 1047, 1047, 966, 944, 875, 839, 823, 809, 751, 728, 708, 663, 638, 619, 567. ¹H NMR (300 MHz, DMSO-*d*₆) δ : 2.29 (s, 3H, CH₃), 7.18–7.24 (m, 2H, CAr-H), 7.31 (d, 2H, 3J = 8.1 Hz, CAr-H),

7.40–7.58 (m, 4H, CAr-H), 7.66 (d, 2H, 3J = 8.1 Hz, CAr-H), 7.75 (d, 1H, 3J = 7.8 Hz, CAr-H), 8.82 (s, 1H, CH=N), 12.36 (s, 1H, NH). Found, %: C 62.09; N 4.28; N 7.32. C₂₀H₁₆F₂N₂O₂S. Calculated, %: C 62.16; N 4.17; N 7.25.

N-[2-[[*E*]-*(2,5*-Difluorophenyl)iminomethyl]phenyl]phenyl]-4-methyl-benzenesulfonamide (**1d**) was prepared from 1.38 g (5 mmol) of 2-*(N*-tosylamino)benzaldehyde and 0.65 g (5 mmol) 2,5-difluoroaniline. The yield is 1.53 g (79%), orange powder, m.p. 170–171 °C (AcOH). IR spectrum (vas. oil), ν , cm⁻¹: 3254 (NH), 1629 m (CH=N), 1603, 1573, 1495, 1463, 1418, 1404, 1378, 1342 s (as SO₂), 1309, 1289, 1273, 1251, 1224, 1166, 1161 s (s SO₂), 1143, 1119, 1091, 1049, 1022, 971, 941, 873, 855, 842, 824, 814, 805, 761, 748, 724, 706, 662, 620, 607, 590, 563. ¹H NMR (300 MHz, DMSO-*d*₆) δ : 2.28 (s, 3H, CH₃), 7.19–7.25 (m, 2H, CAr-H), 7.31 (d, 2H, 3J = 8.4 Hz, CAr-H), 7.36–7.43 (m, 2H, CAr-H), 7.48–7.50 (m, 2H, CAr-H), 7.67 (d, 2H, 3J = 8.4 Hz, CAr-H), 7.76 (d, 1H, 3J = 7.8 Hz, CAr-H), 8.82 (s, 1H, CH=N), 12.22 (s, 1H, NH). Found, %: C 62.07; N 4.25; N 7.36. C₂₀H₁₆F₂N₂O₂S. Calculated, %: C 62.16; N 4.17; N 7.25.

N-[2-[(*E*)-*(2,6*-Difluorophenyl)iminomethyl]phenyl]-4-methyl-benzenesulfonamide (**1e**) was prepared from 1.38 g (5 mmol) of 2-*(N*-tosylamino)benzaldehyde and 0.65 g (5 mmol) of 2,6-difluoroaniline. The yield is 1.78 g (92%), orange powder, m.p. 153–154 °C (AcOH). IR spectrum (vas. oil), ν , cm⁻¹: 3287, 3210, 3127 (NH), 1668, 1625 s (CH=N), 1600, 1572, 1495, 1479, 1470, 1407, 1379, 1343 s (as SO₂), 1311, 1285, 1244, 1221, 1121, 1184, 1171 s (as SO₂), 1157, 1117, 1091, 1047, 1013, 973, 937, 837, 871, 847, 817, 798, 779, 755, 737, 719, 661, 627, 565. ¹H NMR (300 MHz, DMSO-*d*₆) δ : 2.30 (s, 3H, CH₃), 7.21–7.33 (m, 6H, CAr-H), 7.49 (dd, 2H, 3J = 7.5 Hz, 4J = 1.5 Hz, CAr-H), 7.66 (d, 2H, 3J = 8.4 Hz, CAr-H), 7.77 (d, 1H, 3J = 7.5 Hz, CAr-H), 8.87 (s, 1H, CH=N), 11.98 (s, 1H, NH). Found, %: C 62.08; N 4.24; N 7.32. C₂₀H₁₆F₂N₂O₂S. Calculated, %: C 62.16; N 4.17; N 7.25.

N-[2-[[*E*]-*(3,4*-Difluorophenyl)iminomethyl]phenyl]phenyl]-4-methyl-benzenesulfonamide (**1f**) was prepared from 1.38 g (5 mmol) of 2-*(N*-tosylamino)benzaldehyde and 0.65 g (5 mmol) 3,4-difluoroaniline. The yield is 1.69 g (88%), an orange powder, m.p. 174–175 °C (AcOH). IR spectrum (vas. oil), ν , cm⁻¹: 3058 (NH), 1627 m (CH=N), 1600, 1573, 1549, 1514, 1456, 1418, 1399, 1377, 1338 s (as SO₂), 1310, 1292, 1283, 1259, 1217, 1203, 1169 s (as SO₂), 1157, 1140, 1120, 1105, 1090, 1047, 1019, 957, 947, 879, 864, 851, 822, 806, 786, 758, 739, 723, 707, 693, 662, 638, 618, 594, 567. ¹H NMR (300 MHz, DMSO-*d*₆) δ : 2.28 (s, 3H, CH₃), 7.15–7.24 (m, 2H, CAr-H), 7.31 (d, 2H, 3J = 8.1 Hz, CAr-H), 7.40–7.59 (m, 4H, CAr-H), 7.67 (d, 2H, 3J = 8.1 Hz, CAr-H) 7.76 (dd, 1H, 3J = 7.6 Hz, 4J = 1.4 Hz, CAr-H), 8.71 (s, 1H, CH=N), 12.06 (s, 1H, NH). Found, %: C 62.10; N 4.28; N 7.32. C₂₀H₁₆F₂N₂O₂S. Calculated, %: C 62.16; N 4.17; N 7.25.

N-[2-[(*E*)-*(3,5*-Difluorophenyl)iminomethyl]phenyl]-4-methyl-benzenesulfonamide (**1g**) was prepared from 1.38 g (5 mmol) of 2-*(N*-tosylamino)benzaldehyde and 0.65 g (5 mmol) of 3,5-difluoroaniline. The yield is 1.60 g (83%), orange powder, m.p. 146–147 °C (AcOH). IR spectrum (vas. oil), ν , cm⁻¹: 3130, 3088 (NH), 1600 s (CH=N), 1572, 1522, 1503, 1495, 1464, 1454, 1415, 1378, 1346 s (as SO₂), 1323, 1307, 1290, 1251, 1226, 1208, 1187, 1169 s (s SO₂), 1156, 1131, 1119, 1090, 1048, 1020, 1008, 997, 986, 943, 869, 852, 841, 818, 804, 790, 762, 737, 724, 706, 660, 624, 583, 565. ¹H NMR (300 MHz, DMSO-*d*₆) δ : 2.29 (s, 3H, CH₃), 7.03 (dd, 2H, 3J = 8.5 Hz, 4J = 2.2 Hz, CAr-H), 7.15–7.26 (m, 2H, CAr-H), 7.31 (d, 2H, 3J = 8.4 Hz, CAr-H), 7.39 (d, 1H, 3J = 8.1 Hz, CAr-H), 7.48 (tt, 1H, 3J = 8.4 Hz, 4J = 1.5 Hz, CAr-H), 7.66 (d, 2H, 3J = 8.4 Hz, CAr-H), 7.79 (dd, 1H, 3J = 7.8 Hz, 4J = 1.5 Hz, CAr-H), 8.68 (s, 1H, CH=N), 11.75 (s, 1H, NH). Found, %: C 62.07; N 4.28; N 7.33. C₂₀H₁₆F₂N₂O₂S. Calculated, %: C 62.16; N 4.17; N 7.25.

4-Methyl-*N*-[2-[(*E*)-*(2,4,6*-trifluorophenyl)iminomethyl]phenyl]-benzenesulfonamide (**1h**) was prepared from 1.38 g (5 mmol) of 2-*(N*-tosylamino)benzaldehyde and 0.74 g (5 mmol)

2,4,6-trifluoroaniline. The yield is 1.72 g (85%), white powder, m.p. 170–171 °C (AcOH). IR spectrum (vas. oil), ν , cm^{-1} : 3129, 3056 (NH), 1634 s (CH=N), 1613, 1595, 1572, 1486, 1461, 1403, 1379, 1341 s (as SO_2), 1310, 1286, 1237, 1223, 1186, 1171 s (s SO_2), 1155, 1121, 1091, 1048, 1020, 1000, 974, 936, 869, 850, 842, 821, 799, 756, 707, 664, 630, 609, 567. ^1H NMR (300 MHz, $\text{DMSO}-d_6$) δ : 2.30 (s, 3H, CH_3), 7.22 (tt, 1H, $3J = 7.4$ Hz, $4J = 1.5$ Hz, CAr-H), 7.32 (d, 2H, $3J = 8.1$ Hz, CAr-H), 7.37–7.50 (m, 4H, CAr-H), 7.65 (d, 2H, $3J = 8.4$ Hz, CAr-H), 7.78 (dd, 1H, $3J = 8.7$ Hz, $4J = 1.2$ Hz, CAr-H), 8.86 (s, 1H, CH=N), 11.89 (s, 1H, NH). Found, %: C 59.32; N 3.79; N 7.01. $\text{C}_{20}\text{H}_{15}\text{F}_3\text{N}_2\text{O}_2\text{S}$. Calculated, %: C 59.40; N 3.74; N 6.93.

2.2. General Procedure for the Synthesis of Complexes 2a–h

A solution of 0.22 g (1 mmol) of $\text{Zn}(\text{CH}_3\text{COO})_2 \cdot 2\text{H}_2\text{O}$ in 5 mL of methanol was added to a hot solution of 2 mmol azomethine **1a–h** in 30 mL of a mixture of methanol and chloroform (1:1). Further, 0.08 g (2 mmol) of NaOH in 5 mL of methanol were added dropwise. The single crystals of zinc(II) complexes were grown by slow evaporation at the room temperature of their solutions in a mixture of methylene chloride and methanol (1:2).

Bis[2-[(*E*)-(2-fluorophenyl)iminomethyl]-*N*-(*p*-tolylsulfonyl)anilino]zinc(II) (**2a**) was obtained from 0.74 g (2 mmol) of azomethine **1a**. The yield is 0.60 g (75%), yellow powder, m.p. > 300 °C. IR spectrum (vas. oil), ν , cm^{-1} : 1615 s (CH=N), 1605, 1555, 1480, 1461, 1403, 1377, 1300 s (as SO_2), 1284, 1266, 1207, 1172, 1139 s (s SO_2), 1104, 1081, 1056, 954, 932, 901, 861, 846, 833, 812, 787, 756, 722, 666, 617, 594, 567. ^1H NMR (300 MHz, $\text{DMSO}-d_6$) δ : 2.28 (s, 3H, CH_3), 6.90 (t, 1H, $3J = 6.3$ Hz, CAr-H), 7.10–7.33 (m, 7H, CAr-H), 7.39 (t, 1H, $3J = 7.8$ Hz, CAr-H), 7.65–7.73 (m, 3H, CAr-H), 8.74 (s, 1H, CH=N). Found, %: C 59.96; H 4.15; N 7.09; Zn 8.10. $\text{C}_{40}\text{H}_{32}\text{F}_2\text{N}_4\text{O}_4\text{S}_2\text{Zn}$. Calculated, %: C 60.04; H 4.03; N 7.00; Zn 8.17.

Bis[2-[(*E*)-(4-fluorophenyl)iminomethyl]-*N*-(*p*-tolylsulfonyl)anilino]zinc(II) (**2b**) was prepared from 0.74 g (2 mmol) of azomethine **1b**. The yield is 0.58 g (73%), yellow powder, m.p. > 300 °C. IR spectrum (vas. oil), ν , cm^{-1} : 1613 s (CH=N), 1598, 1556, 1504, 1480, 1464, 1446, 1399, 1377, 1297 s (as SO_2), 1287, 1258, 1233, 1176, 1138 s (s SO_2), 1081, 1056, 1022, 955, 905, 902, 880, 856, 833, 813, 780, 758, 713, 666, 645, 619, 585, 560. ^1H NMR (300 MHz, $\text{DMSO}-d_6$) δ : 2.30 (s, 3H, CH_3), 6.92–6.96 (m, 1H, CAr-H), 7.15–7.22 (m, 4H, CAr-H), 7.32–7.36 (m, 4H, CAr-H), 7.65 (d, 2H, $3J = 8.1$ Hz, CAr-H), 7.74 (d, 1H, $3J = 7.8$ Hz, CAr-H), 8.74 (s, 1H, CH=N). Found, %: C 60.00; H 4.14; N 6.91; Zn 8.10. $\text{C}_{40}\text{H}_{32}\text{F}_2\text{N}_4\text{O}_4\text{S}_2\text{Zn}$. Calculated, %: C 60.04; H 4.03; N 7.00; Zn 8.17.

Bis[2-[(*E*)-(2,4-difluorophenyl)iminomethyl]-*N*-(*p*-tolylsulfonyl)anilino] zinc(II) (**2c**) was prepared from 0.77 g (2 mmol) of azomethine **1c**. The yield is 0.60 g (72%), yellow powder, m.p. > 300 °C. IR spectrum (vas. oil), ν , cm^{-1} : 1613 s (CH=N), 1556, 1503, 1482, 1462, 1445, 1402, 1377, 1301 s (as SO_2), 1283, 1264, 1219, 1172, 1139 (s SO_2), 1097, 1081, 1022, 1007, 970, 954, 933, 933, 898, 850, 842, 813, 757, 738, 713, 665, 646, 611, 578. ^1H NMR (300 MHz, $\text{DMSO}-d_6$) δ : 2.27 (s, 3H, CH_3), 6.91 (t, 1H, $3J = 7.1$ Hz, CAr-H), 7.04 (t, 1H, $3J = 7.5$ Hz, CAr-H), 7.17 (d, 2H, $3J = 7.8$ Hz, CAr-H), 7.21–7.30 (m, 3H, CAr-H), 7.43 (q, 1H, $3J = 6.3$ Hz, CAr-H), 7.66 (d, 1H, $3J = 7.5$ Hz, CAr-H), 7.77 (d, 2H, $3J = 7.8$ Hz, CAr-H), 8.74 (s, 1H, CH=N). Found, %: C 57.40; H 3.69; N 6.75; Zn 7.72. $\text{C}_{40}\text{H}_{30}\text{F}_4\text{N}_4\text{O}_4\text{S}_2\text{Zn}$. Calculated, %: C 57.45; H 3.62; N 6.70; Zn 7.82.

Bis[2-[(*E*)-(2,5-difluorophenyl)iminomethyl]-*N*-(*p*-tolylsulfonyl)anilino]zinc(II) (**2d**) was prepared from 0.77 g (2 mmol) of azomethine **1d**. The yield is 0.57 g (68%), yellow powder, m.p. 289–290 °C. IR spectrum (vas. oil), ν , cm^{-1} : 1603 s (CH=N), 1553, 1525, 1495, 1481, 1463, 1454, 1434, 1409, 1377, 1338, 1302 s (as SO_2), 1290, 1263, 1207, 1193, 1148, 1134 s (s SO_2), 1100, 1081, 1061, 1021, 1011, 969, 942, 895, 895, 874, 842, 822, 814, 786, 758, 734, 711, 664, 643, 610, 574, 552. ^1H NMR (300 MHz, $\text{DMSO}-d_6$) δ : 2.27 (s, 3H, CH_3), 6.92 (t, 1H, $3J = 7.2$ Hz, CAr-H), 7.09–7.34 (m, 7H, CAr-H), 7.67 (d, 1H, $3J = 7.8$ Hz, CAr-H), 7.77 (d, 2H, $3J = 8.1$ Hz, CAr-H), 8.77 (s, 1H, CH=N). Found, %: C 57.39; H 3.68; N 6.74; Zn 7.89.

$C_{40}H_{30}F_4N_4O_4S_2Zn$. Calculated, %: C 57.45; H 3.62; N 6.70; Zn 7.82.

Bis[2-[(*E*)-(2,6-difluorophenyl)iminomethyl]-*N*-(*p*-tolylsulfonyl)anilino]zinc(II) (**2e**) was prepared from 0.77 g (2 mmol) of azomethine **1e**. The yield is 0.64 g (77%), yellow powder, m.p. > 300 °C. IR spectrum (vas. oil), ν , cm^{-1} : 1615 s (CH=N), 1603, 1552, 1476, 1441, 1413, 1377, 1301 s (as SO₂), 1287, 1263, 1242, 1182, 1172, 1140 s (s SO₂), 1081, 1055, 1017, 982, 946, 896, 849, 827, 811, 772, 757, 738, 713, 663, 642, 617, 598, 578. ¹H NMR (300 MHz, DMSO-*d*₆) δ : 2.24 (s, 3H, CH₃), 6.87–7.25 (m, 8H, CAr-H), 7.64–7.86 (m, 3H, CAr-H), 8.84 (s, 1H, CH=N). Found, %: C 57.40; H 3.69; N 6.75; Zn 7.76. $C_{40}H_{30}F_4N_4O_4S_2Zn$. Calculated, %: C 57.45; H 3.62; N 6.70; Zn 7.82.

Bis[2-[(*E*)-(3,4-difluorophenyl)iminomethyl]-*N*-(*p*-tolylsulfonyl)anilino]zinc(II) (**2f**) was prepared from 0.77 g (2 mmol) of azomethine **1f**. The yield is 0.59 g (70%), yellow powder, m.p. > 300 °C. IR spectrum (vas. oil), ν , cm^{-1} : 1599 s (CH=N), 1555, 1510, 1479, 1464, 1448, 1396, 1377, 1300 s (as SO₂), 1263, 1199, 1177, 1135 s (s SO₂), 1112, 1081, 1057, 1023, 974, 947, 895, 864, 839, 814, 788, 756, 723, 708, 666, 635, 620, 578. ¹H NMR (300 MHz, DMSO-*d*₆) δ : 2.30 (s, 3H, CH₃), 6.96 (t, 1H, 3J = 7.2 Hz, CAr-H), 7.12–7.20 (m, 3H, CAr-H), 7.29–7.48 (m, 4H, CAr-H), 7.69 (d, 2H, 3J = 8.4 Hz, CAr-H), 7.74 (d, 1H, 4J = 1.5 Hz, CAr-H), 8.73 (s, 1H, CH=N). Found, %: C 57.40; H 3.68; N 6.95; Zn 7.88. $C_{40}H_{30}F_4N_4O_4S_2Zn$. Calculated, %: C 57.45; H 3.62; N 6.70; Zn 7.82.

Bis[2-[(*E*)-(3,5-difluorophenyl)iminomethyl]-*N*-(*p*-tolylsulfonyl)anilino]zinc(II) (**2g**) was prepared from 0.77 g (2 mmol) of azomethine **1g**. The yield is 0.66 g (79%), yellow powder, m.p. > 300 °C. IR spectrum (vas. oil), ν , cm^{-1} : 1601 s (CH=N), 1555, 1519, 1486, 1468, 1456, 1420, 1377, 1326, 1299 s (as SO₂), 1263, 1220, 1207, 1186, 1152, 1131 s (s SO₂), 1081, 1062, 1041, 1016, 988, 968, 944, 894, 867, 846, 835, 822, 756, 721, 710, 679, 663, 646, 624, 567. ¹H NMR (300 MHz, DMSO-*d*₆) δ : 2.30 (s, 3H, CH₃), 6.95–7.02 (m, 3H, CAr-H), 7.17–7.30 (m, 4H, CAr-H), 7.37 (tt, 1H, 3J = 8.4 Hz, 4J = 1.2 Hz, CAr-H), 7.71 (d, 2H, 3J = 8.1 Hz, CAr-H), 7.74 (s, 1H, CAr-H), 8.77 (s, 1H, CH=N). Found, %: C 57.40; H 3.72; N 6.78; Zn 7.88. $C_{40}H_{30}F_4N_4O_4S_2Zn$. Calculated, %: C 57.45; H 3.62; N 6.70; Zn 7.82.

Bis[*N*-(*p*-tolylsulfonyl)-2-[(*E*)-(2,4,6-trifluorophenyl)iminomethyl]anilino]zinc(II) (**2h**) was prepared from 0.81 g (2 mmol) of azomethine **1h**. The yield is 0.67 g (77%), yellow powder, m.p. > 300 °C. IR spectrum (vas. oil), ν , cm^{-1} : 1610 s (CH=N), 1556, 1501, 1479, 1454, 1441, 1406, 1377, 1358, 1302 s (as SO₂), 1280, 1266, 1230, 1181, 1141 s (s SO₂), 1119, 1084, 1047, 1021, 992, 998, 954, 898, 898, 862, 836, 826, 767, 757, 730, 709, 667, 645, 610, 579, 554. ¹H NMR (300 MHz, DMSO-*d*₆) δ : 2.23 (s, 3H, CH₃), 6.88 (t, 1H, 3J = 7.2 Hz, CAr-H), 7.16 (d, 4H, 3J = 8.1 Hz, CAr-H), 7.22–7.31 (m, 2H, CAr-H), 7.62 (d, 1H, 3J = 6.9 Hz, CAr-H), 7.90 (d, 2H, 3J = 7.8 Hz, CAr-H), 8.85 (s, 1H, CH=N). Found, %: C 55.01; H 3.29; N 6.47; Zn 7.38. $C_{40}H_{28}F_6N_4O_4S_2Zn$. Calculated, %: C 55.08; H 3.24; N 6.42; Zn 7.50.

3. Results

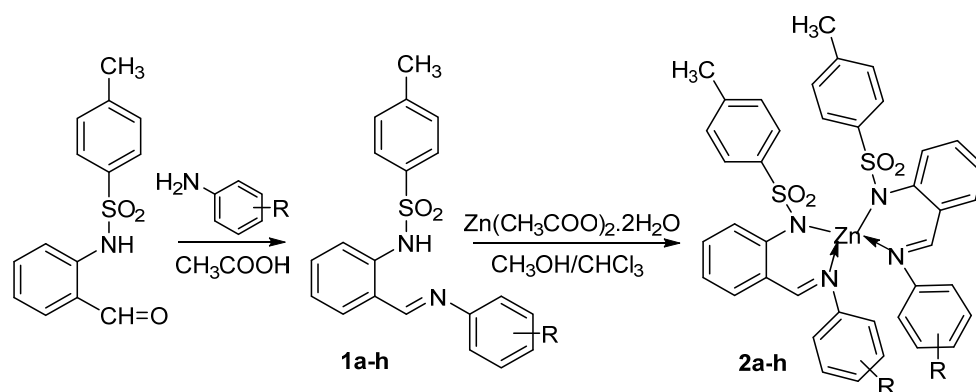
3.1. Synthesis and Spectroscopic Studies of Azomethines **1a–h** and Zinc(II) Complexes **2a–h**

The synthesis of azomethines **1a–h** and zinc complexes **2a–h** on their basis is presented in Scheme 1.

The IR spectra of azomethines **1a–h** show weakly intense ν NH absorption bands in the region of 3058–3287 cm^{-1} and ν CH=N absorption bands in the region of 1600–1634 cm^{-1} , $\nu_{as}SO_2$ 1338–1346 cm^{-1} and ν_sSO_2 1161–1171 cm^{-1} . The azomethines **1a–h** ¹H NMR spectra contain the proton signals of NH groups at 11.75–12.46 ppm and the CH=N group's proton signals at 8.68–8.87 ppm.

By the reaction of azomethine **1a–h** and zinc acetate dihydrate (molar ratio of ligand: zinc acetate is 2:1), we obtained the complexes **2a–h**. These complexes are yellow crystalline substances with an m.p. of >300 °C and soluble in methylene chloride, DMFA, and DMSO. The composition of the complexes is ZnL₂ according to the elemental analysis data. The

absorption bands of the νNH ligand disappear in the IR spectra of the complexes. The absorption bands of $\nu\text{CH}=\text{N}$ undergo a shift to the long wavelength (low frequency) region by $8\text{--}28\text{ cm}^{-1}$ and the bands of νasSO_2 by $38\text{--}47\text{ cm}^{-1}$ and νsSO_2 by $22\text{--}28\text{ cm}^{-1}$. The formation of zinc complexes is also indicated by the disappearance of the NH group of ligands **1a–h** signal in the ^1H NMR spectra. In addition, the signals of the CH=N group's protons are shifted slightly to the strong field, which is typical for the formation of chelate structures [20,21].



R = 2- F (**1a,2a**); R = 4- F (**1b,2b**); R = 2,4- F₂ (**1c,2c**); R = 2,5- F₂ (**1d,2d**);
R = 2,6- F₂ (**1e,2e**); R = 3,4- F₂ (**1f,2f**); R = 3,5- F₂ (**1g,2g**); R = 2,4,6- F₃ (**1h,2h**)

Scheme 1. Synthesis of azomethines **1a–h** and complexes **2a–h**.

3.2. Crystal Structures of **1d,f**

The molecular structures of **1d** and **1f** are shown in Figure 1.

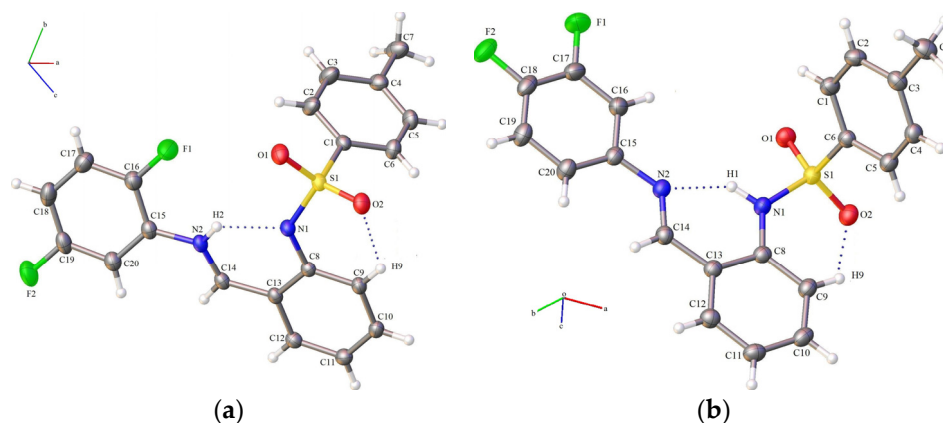


Figure 1. Molecular structures of **1d** (a) and **1f** (b). Displacement ellipsoids are shown at the 50% probability level. The dashed bonds correspond to N–H...N and C–H...O=S intramolecular hydrogen bonds.

Crystal **1d**, unlike crystal **1f**, consists of two crystallographically independent molecules. The geometric parameters for all molecules (Table 1) are within the typical ranges observed for other Schiff base ligands with tosylamine fragments [23,24]. Each iminomethylphenyl fragment is planar, where the angles between the planes are about 2° . The angles between benzene cycles of the tosylamine fragments and the iminomethylphenyl fragments are close to orthogonal ($82.89(6)^\circ$ and $89.38(6)^\circ$ for **1d**, $78.28(9)^\circ$ for **1f**). The angles between the iminomethylphenyl fragment and the plane of the fluorine-substituted aniline fragment in **1d** are $19.63(5)^\circ$ and $14.37(6)^\circ$, while, in **1f**, these angles are much smaller and equal to about $4.74(4)^\circ$. All the polyhedron's angles are close to ideal tetrahedral geometry, except the angle $\text{O1}=\text{S1}=\text{O2}$ (119.7°). The $\text{S1}=\text{O1}$ and $\text{S1}=\text{O2}$ bond distances in azomethines **1d**

and **1f** are very close and range from 1.5209(2) to 1.5278(1) Å. The S1-N1 bond lengths, 1.7267(1)–1.7366(2) Å, are very close to the single bond lengths (1.74 Å).

Table 1. Main bond lengths and angles in **1d,f**.

Compound/Parameter	1d	1f
Bond Distances, Å		
N1-S1/N1A-S1A	1.7366(2), 1.7327(2)	1.7267(1)
C1-S1/C1A-S1A	1.8782(2), 1.8719(2)	1.8765(2)
N1-C8/N1A-C8A	1.5061(2), 1.4945(3)	1.4931(2)
O1-S1/O1A-S1A	1.5265(2)/1.5258(2)	1.5250(2)
O2-S1/O2A-S1A	1.5209(2)/1.5240(2)	1.5278(1)
N2-C14/N2A-C14A	1.3574(2), 1.3594(3)	1.3644(2)
N2-C15/N2A-C15A	1.4980(3), 1.4990(3)	1.5060(2)
Angles, deg.		
C1-S1-N1/C1A-S1A-N1A	106.22(9), 105.77(9)	106.43(7)
C8-N1-S1/C8A-N1A-S1A	127.24(1), 127.65(1)	129.89(9)
O1-S1-O2/O1A-S1A-O2A	119.71(9), 119.78(9)	119.69(7)
C14-N2-C15/C14A-N2A-C15A	123.07(2), 121.60(2)	121.87(1)
Torsion Angles, deg.		
C1-S1-N1-C8/C1A-S1A-N1A-C8A	67.38(2), 73.58(2),	80.99(9)
C13-C14-N2-C15/C13A-C14A-N2A-C15A	175.57(2), 179.19(2)	177.55(2)

The molecular structures of each ligand **1d,f** contain two specific intramolecular interactions (Figure 2). One of them, an intramolecular hydrogen bond N–H...N, differs significantly for these two compounds. The H-bonds in the crystal of **1d** are formed as N2–H2...N1, with bond lengths 2.098 and 2.119 Å; while in **1f**, this bond is due to N1–H1...N2 and is much shorter than 1.999 Å (Table 2). The existence of such strong hydrogen bonds in the molecules of azomethines **1d,f** leads to the formation of an almost planar bicyclic iminomethylphenyl system, significantly increasing their structural rigidity [25]. The second specific interaction is the intramolecular hydrogen bond C9–H...O2=S1 contact with interatomic distances of 2.477 and 2.537 Å in **1d** and 2.564 Å in **1f**, respectively (Table 2).

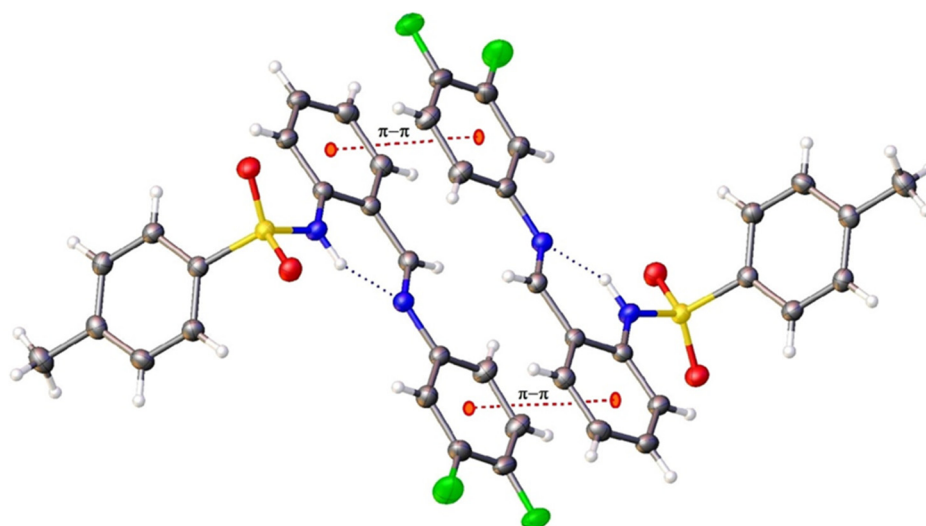


Figure 2. The antiparallel π -stacking interactions in compound **1f**.

Table 2. Parameters of H-bonds in crystals of **1d,f**.

Compound/Parameter	H-Bond	D-H, Å	H...A, Å	D...A, Å	D-H...A, deg.
1d	N2-H2...N1	0.880(3)	2.098(2)	2.806(2)	136.98(3)
	N2A-H2A...N1A	0.880(3)	2.119(3)	2.815(3)	135.53(3)
	C9-H9...O2	0.95	2.537(3)	3.214(3)	128.40(3)
	C9A-H9A...O2A	0.95	2.477(3)	3.159(3)	128.65(3)
	C5A-H5A...O4Aa	0.95	2.711(3)	3.530(3)	144.80(3)
	C7A-H7A...O4Aa	0.95	2.691(3)	3.600(3)	154.37(3)
	C17-H17...O1Ab	0.95	2.651(3)	3.377(3)	133.52(3)
1f	N1-H1...N2	0.953(2)	1.999(2)	2.808(19)	141.59(2)
	C9-H9...O2	0.95	2.564(2)	3.198(2)	124.37(2)
	C4-H4...O1Aa	0.95	2.685(2)	3.580(2)	159.14(2)

Symmetry equivalent: a – 1 + x,y,z; b – x, 1 – y, 1 – z.

The crystal packing of molecule **1d** is due to intermolecular hydrogen bonds between the oxygen atoms of the tosylamine group of the ligand of one of the molecules and the hydrogen atom of the fluorine-substituted aniline fragment, with the H-bond length 2.651 Å, and the methyl group of the tosylamine fragment, with the H-bond length 2.691 Å of neighboring molecules (Table 2). The result of such interactions is the formation of infinitely elongated chains along the [b] direction in the crystal. Crystal **1d** also exhibits π -stacking interactions between the rings of fluorine-substituted aniline fragments, with centroid distances of 3.964 Å, and the rings of iminomethylphenyl fragments, with centroid distances of 4.049 Å of neighboring molecules.

The crystal packing of molecule **1f** is determined by intermolecular hydrogen bonds between the oxygen atoms of the tosylamine group of the ligand and the tosylamine fragment of the neighboring molecule with an H-bond length of 2.685 Å. Owing to antiparallel π -stacking interactions of rings of iminomethylphenyl and fluorine-substituted aniline fragments, the stacks of molecules elongated in the [a] direction are formed (Figure 2).

3.3. X-ray Absorption Spectroscopy of Zinc(II) Complexes **2a–h**

The XANES and EXAFS X-ray absorption spectroscopy of the Zn K absorption edges was used to characterize the local atomic environment of zinc ions in complexes **2a–h**. Figure 3 shows normalized XANES and the corresponding MFT (Modules of Fourier Transform) EXAFS for all zinc(II) complexes **2a–h**. It is known that the X-ray absorption edge depends both on the oxidized state of the metal ion and on the chemical environment, viz., effective charge, nature of ligands, coordination numbers, electronegativity of anions, and covalent character of the bonds surrounding the metal ion. The absorption edge and white-line position's characteristics of the spectral features of the Zn K absorption edges for **2a–h** are similar (Figure 3a), indicating a similar environment of zinc ions in these compounds. In the XANES spectra of complexes **2a–h**, there is no pre-edge peak A due to the filled 3d shell of Zn(II). The energy positions of intense peak C (white line) correspond to the maximum of the X-ray absorption spectrum. And, the postedge peak D has some differences in the case of complexes **2e** and **2h**, where fluorine atoms are in the 2,6 positions of the aniline fragment of ligands.

The main characteristics of the coordination polyhedron for complexes **2a–h** were determined by EXAFS analysis. The EXAFS MFTs of these compounds are shown in Figure 3b. All the MFTs have a main peak at $r = 1.51\text{--}1.53$ Å, which corresponds to the photoelectron wave scattering by the nearest coordination sphere (CS) of the nitrogen atoms of the ligands. The MFT peaks at larger values of $r > 2.5$ Å are associated with the subsequent CSs containing different ligand atoms, mainly carbon atoms, as well as oxygen and sulfur tosylamine fragments of the ligands. It can be noted that, in the MFT of complexes **2e** and **2h** at $r = 2.85\text{--}2.90$ Å, there is a peak of high amplitude, which we interpreted as a manifestation of photoelectron scattering on fluorine atoms in the two and six positions of the aniline fragment of the ligands. The EXAFS model's calculations show

that the nearest environment of zinc ions in all **2a–h** complexes is similar and consists of four nitrogen atoms with average distances of Zn...N about 1.97–1.99 Å and 2.02–2.05 Å (Table 3). The obtained values of the Debye–Waller coefficients were about 0.0030 Å², which agrees with similar values for the analogous complexes determined earlier [10,11].

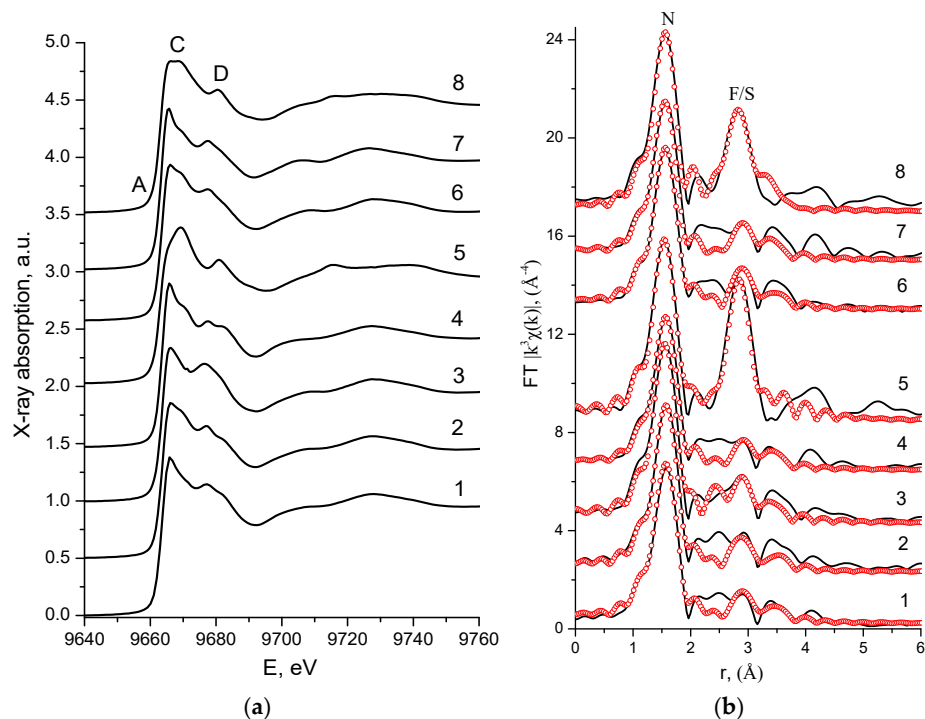


Figure 3. Normalized XANES spectra (a) and MFT EXAFS (b) of Zn K edges for the complexes **2a** (1), **2b** (2), **2c** (3), **2d** (4), **2e** (5), **2f** (6), **2g** (7), and **2h** (8) experiment—solid black line, best-fit theory—empty red circles.

Table 3. Parameters¹ of the local structure around the zinc ions in complexes **2a–h**, obtained from EXAFS analysis of Zn K-edges.

Compound	Bond	N	R, Å	σ^2 , Å ²	Q, %
2a	Zn–N	2	1.99	0.0030	1.3
	Zn–N	2	2.03	0.0030	
2b	Zn–N	2	2.00	0.0030	1.5
	Zn–N	2	2.04	0.0030	
2c	Zn–N	2	1.97	0.0030	1.4
	Zn–N	2	2.02	0.0030	
2d	Zn–N	2	1.98	0.0030	1.0
	Zn–N	2	2.05	0.0030	
2e	Zn–N	2	1.98	0.0030	3.9
	Zn–N	2	2.01	0.0030	
2f	Zn–F	2	3.24	0.0035	1.4
	Zn–N	2	1.98	0.0034	
2g	Zn–N	2	2.04	0.0034	1.6
	Zn–N	2	1.97	0.0032	
2h	Zn–N	2	2.04	0.0032	4.6
	Zn–N	2	1.98	0.0030	
	Zn–F	2	3.20	0.0035	

¹ N—coordination number, R—interatomic distance, σ^2 —Debye–Waller factor, and Q—is the integral fit quality factor of EXAFS fitting: $\Delta r = 1.00$ – 1.98 Å.

3.4. A Single-Crystal X-ray Diffraction of Zinc(II) Complexes **2d**,**h**,**f**

Single-crystal X-ray diffraction analysis revealed that complexes **2d**,**h** crystallized in the monoclinic space group $C2/c$, whereas complex **2f** crystallized in the triclinic space group $P-1$, respectively. The summary of selected bond lengths and angles for the molecules in the complexes are shown in Table 4. The molecular geometries of the complexes **2d**,**h**,**f** were quite similar, as depicted in Figures 4–6.

Table 4. Main bond lengths and angles in **2d**,**h**,**f**.

Compound/Parameter	2d	2h	2f	
Bond Distances, Å				
Zn—N1	2.0561(19)	2.0396(11)	Zn1—N1	2.0566(16)
Zn—N1ai	2.0561(19) i	2.0396(11) i	Zn1—N2	2.0589(14)
Zn—N2	1.9857(19)	1.9938(11)	Zn1—N3	1.9863(14)
Zn—N2ai	1.9857(19) i	1.9938(11) i	Zn1—N4	1.9904(14)
S1—O1	1.4409(19)	1.4412(11)	S1—O1	1.4450(13)
S1—O2	1.4504(17)	1.4558(11)	S1—O2	1.4521(13)
Angles, deg.				
N2—Zn1—N2a	139.97(11)	145.68(7)	N3—Zn1—N4	149.27(6)
N2—Zn1—N1	113.23(8)	103.98(5)	N2—Zn1—N4	103.73(6)
N2a—Zn1—N1a	113.22(8)	103.98(5)	N1—Zn1—N3	110.13(6)
N2—Zn1—N1a	93.22(8)	93.21(5)	N1—Zn1—N4	91.17(7)
N1—Zn1—N2a	93.22(8)	93.21(5)	N2—Zn1—N3	90.83(6)
N1—Zn1—N1a	97.68(11)	119.44(7)	N1—Zn1—N2	107.96(6)
Torsion Angles, deg.				
C14—S1—N2—C13	68.80(3)	62.92(3)	C27—S1—N3—C14	63.05(14)
C14a—S1a—N2a—C13ai	68.80(3)	62.92(3)	C34—S2—N4—C13	69.41(15)
C8—C7—N1a—C4a	174.62(3)	176.45(3)	C8—C7—N1—C6	178.55(3)
C8a—C7a—N1—C4i	174.62(3)	176.45(3)	C19—C20—N2—C21	178.18(3)

Symmetry equivalent: (i) $-x + 1, y, -z + 1/2$.

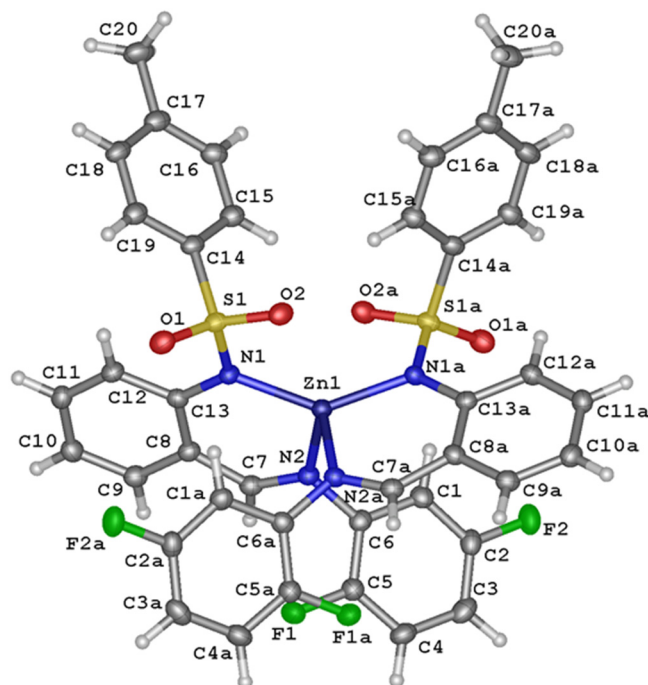


Figure 4. A view of the structure of complex **2d**, showing the atom-labeling scheme. Displacement ellipsoids are drawn at the 50% probability level. Symmetry equivalent: (a) $1 - x, y, 1/2 - z$.

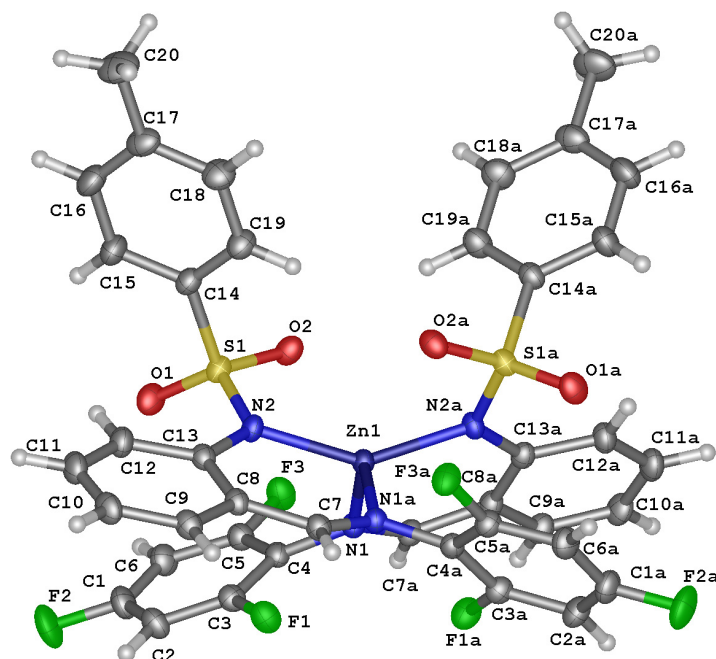


Figure 5. A view of the structure of complex **2h**, showing the atom-labeling scheme. Displacement ellipsoids are drawn at the 50% probability level. Symmetry equivalent: (a) $1 - x, y, 3/2 - z$.

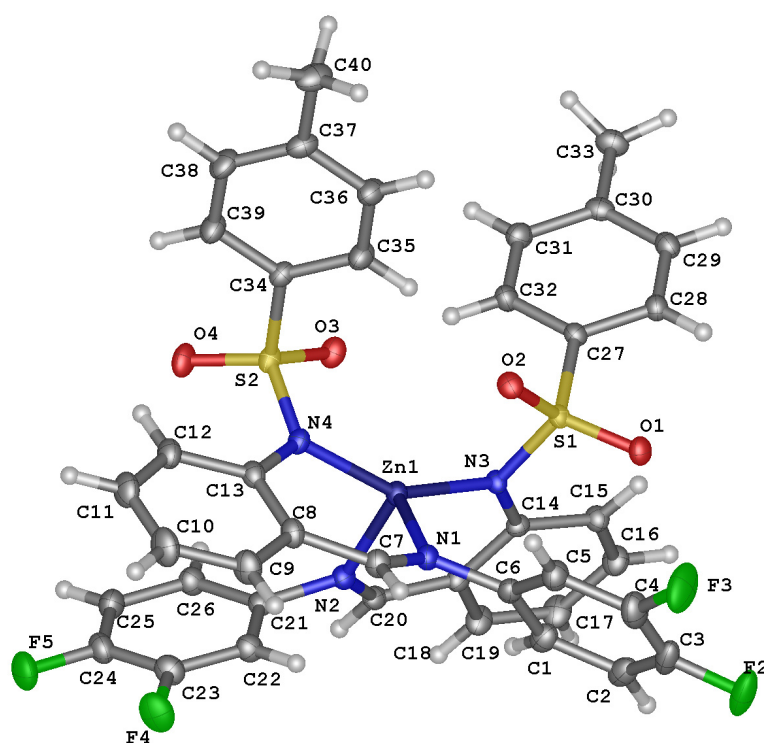


Figure 6. A view of the structure of complex **2f**, showing the atom-labeling scheme. Displacement ellipsoids are drawn at the 50% probability level.

The compounds **2d,h** form centrosymmetric mononuclear molecules with two Schiff base ligands. In all three complexes, the zinc ions have an oxidation state of 2+ and a bi-capped tetrahedral coordination environment “4 + 2” by four N atoms from the tosylamine and imine groups [Zn1-N2 1.9857(19) Å, Zn1-N1 2.0561(19) Å for **2d**, Zn1-N2 1.9938(11) Å, Zn1-N1 2.0396(11) Å for **2h**, and Zn1-N3,N4 1.9865(15) Å, 1.9905(15) Å, Zn1-N1,N2 2.0564(17), 2.0597(16) Å for **2h**] and additional weaker interactions with two O atoms from

the sulfo groups [Zn1...O2,O2a 2.670 Å, and 2.719 Å for **2d,h**, and Zn1...O2 2.590 Å, and Zn1...O3 2.653 Å for **2f**]. The average values of the bond lengths coincide with the average values of such bonds from the CSD for similar complexes [20,21,26]. The bond lengths obtained by XRD show good agreement with the EXAFS data of the relative compounds. The bond angles N-Zn1-N in the coordination sphere of complexes **2d,h,f** vary in the interval from 90.81 to 149.28 deg., and, therefore, the zinc coordination polyhedron in these compounds can be described as a distorted tetrahedron. The angular structural parameter τ_4 for the four coordinate complexes [27] was equal to 0.76 (**2d**), 0.67 (**2h**), and 0.73 (**2f**), which fits with a seesaw description.

The crystal packing of complex **2d** is enhanced by intermolecular hydrogen bonds C18-H18...F2, C16-H16...F1 of fluorine atoms of a fluorine-substituted aniline fragment and benzene cycles of tosylamine fragments, as well as between oxygen atoms of the sulfo group of one of the tosylamine fragments with the methyl group of the tosylamine fragment of neighboring molecule C20-H20B...O1 (Table 5).

Table 5. Parameters of H-bonds in crystals of **2d,h,f**.

Compound	H-Bond	D-H, Å	H...A, Å	D...A, Å	D-H...A, deg.
2d	C18-H18...F2	0.95	2.552	3.410	151.11
	C16-H16...F1	0.95	2.591	3.136	116.80
	C20-H20B...O1	0.98	2.579	3.497	156.02
2h	O3-H3...O2	0.84	2.030	2.861	170.19
	C6-H7...O3	0.95	2.375	3.298	163.77
	C9-H9...O3	0.95	2.655	3.523	152.09
	C6-H6...F2	0.95	2.578	3.315	134.69
2f	C10-H10...F2	0.95	2.330	3.273	171.86
	C5-H5A...F4	0.84	2.340	3.130	157.04
	O5-H5A...F5	0.84	2.402	3.034	132.60
	C18-H18...O1	0.95	2.410	3.260	149.78
	C2-H2...O5	0.95	2.416	3.328	160.73
	C22-H22...F2	0.95	2.421	3.266	148.08
	C33-H33A...O3	0.98	2.560	3.527	168.98
	C7-H7...O5	0.95	2.577	3.522	172.93
	C26-H26...O2	0.95	2.594	3.275	128.94
C11-H11...O1	0.95	2.602	3.458	150.11	

In contrast to the crystalline packing of complex **2d**, the crystal lattice of complex **2h** contains a methanol solvate molecule that forms with the complex H-bonds molecule with iminomethylphenyl fragments C6-H7...O3, C9-H9...O3, and O3-H3...O2 with the sulfo group of the tosylamine fragment of the ligand. Intermolecular interactions C6-H6...F2, and the interactions between the two fluorine-substituted aniline fragments of the ligands, are also present (Table 5).

As in the crystal of complex **2h**, in the unit cell **2f**, there is a solvate molecule, methanol, which forms hydrogen bonds O5-H5A...F5 and C5-H5A...F4 with fluorine-substituted aniline fragments of ligands in the molecules of the complex. Fluorine of the (phenyl)iminomethyl fragments has two conformational positions with different occupancies, which were defined separately. In the case of conformation “part 2”, F1 is too close to the O5 atom of methanol (2.005 Å). Thus, the methanol molecule is present in the structure of **2f** only in the case of conformation “part 1”. Thus, the fractional chemical formula $C_{40}H_{30}F_4N_4O_4S_2Zn, 0.632(CH_4O)$ is a consequence of the fractional population of methanol. In addition, hydrogen bonds are formed between the oxygen atoms of the sulfo group with the phenyl ring of the aldehyde fragment and the phenyl ring of the tosylamine fragment of ligands.

The crystal structure of **2f** is strengthened by π - π interactions between benzene rings of the tosyl fragments of ligands with centroid–centroid distances of 3.779 Å and 3.821 Å

and shift distances of 1.419 and 1.060 Å, respectively. Moreover, π - π interactions between rings of fluorine-substituted aniline fragments with centroid distances of 3.618 Å and a shift distance of 1.261 Å, increasing the stability of crystals, are present.

3.5. The Photoluminescent Properties

The luminescent properties of azomethine **1a–f** and Zn complexes **2a–f** were studied both in the solid state and a dichloromethane solution at room temperature. The data are depicted in Table 6. In the solid state, the parent ligands exhibit orange–red luminescence in the form of broad band luminescence with maxima at 586–598 nm, respectively, which can be attributed to the π^* - π transitions.

Table 6. PL data of **1a–h** and **2a–g** in CH_2Cl_2 and solid state at 293 K.

Compound	Solid				CH_2Cl_2		
	λ_{max} (nm)	QY %	Lifetime (ns)	CIE	λ_{max} (nm)	QY %	Lifetime (ns)
1a	580	25.75	3.7	0.526; 0.476	-	-	-
1b	579	43.89	3.8	0.489; 0.509	-	-	-
1c	572	23.59	3.4	0.507; 0.499	-	-	-
1d	577	17.00	3.7	0.540; 0.458	-	-	-
1e	572	25.36	3.2	0.504; 0.500	-	-	-
1f	581	16.36	3.5	0.532; 0.466	-	-	-
1g	589	10.33	3.2	0.546; 0.435	-	-	-
1h	567	15.12	3.4	0.492; 0.511	-	-	-
2a	485	31.98	7.1	0.170; 0.376	480	2.35	3.7
2b	484	31.34	6.7	0.162; 0.371	481	2.24	3.5
2c	491	37.0	6.6	0.181; 0.432	481	0.50	3.0
2d	475	40.59	6.9	0.173; 0.310	493	0.95	3.5
2e	506	22.31	6.5	0.230; 0.490	473	1.05	3.8
2f	499	42.18	6.2	0.232; 0.528	491	2.64	3.7
2g	476	34.49	6.8	0.165; 0.321	504	0.88	3.6
2h	475	18.5	9.1	0.169; 0.260	473	4.8	3.5

The Zn complexes exhibit intense luminescence upon excitation, with a wavelength of 380–400 nm. The emission spectrum of the solid samples has the appearance of a broad band, with maxima in the range from 475 to 506 nm and the same maxima in a solution ranging from 473 to 504 nm. It is noteworthy that the emission bands of the complexes are hypsochromically shifted relative to the emission bands of the corresponding ligands. (Figure 7). In addition, it is noteworthy that the introduction of a fluorine atom into the *meta* position leads to a bathochromic shift of the emission band, while the introduction into the *ortho* or *para* position, with respect to the azomethine group, leads to a hypsochromic shift which is well seen for the spectra of complexes in solutions in which intermolecular effects are absent (Figure 8). This is consistent with the combined effect of the electron-donor azomethine group and electron-acceptor fluorine atom, leading to an increase in the energy difference of the frontier molecular orbitals when fluorine atoms are introduced into *ortho/para* positions and the opposite effect in the case of metasubstitution.

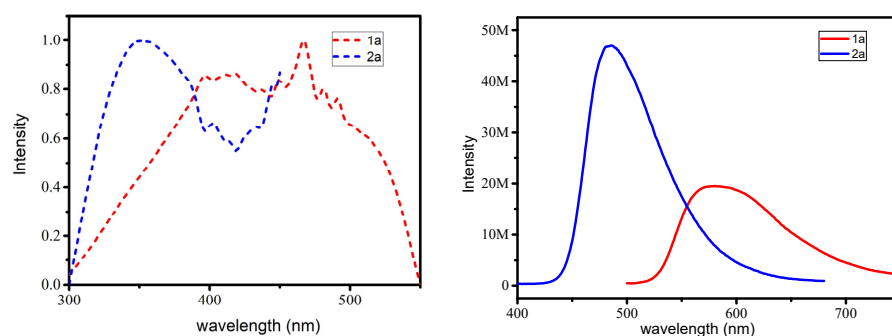


Figure 7. Comparable normalized excitation (left) and photoluminescent (right) spectra of free ligand **1a** (red line) and related complex **2a** (blue line) of the solid state.

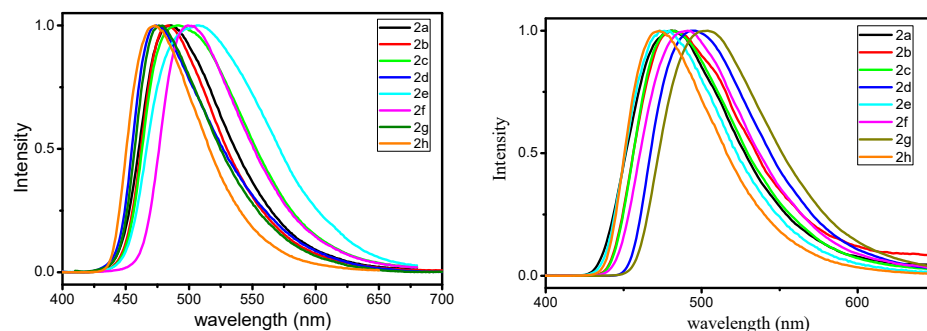


Figure 8. Normalized PL spectra of the solid state (**left**) and CH₂Cl₂ solution (10⁻⁴ M) (**right**) of complexes **2a–h**.

Solid-state complexes **2a–h** exhibit blue or greenish-blue luminescence, which makes them promising materials for OLED devices. The chromaticity coordinates (CIE 1932) are presented in Table 6. The PL spectra of zinc complexes recorded in dichloromethane solution show fluorescence of moderate intensity. The emission maxima are in the region of 473–511 nm.

The luminescence QYs of the complexes in a CH₂Cl₂ solution were measured by the relative method using quinine sulfate (QY = 0.546) as a reference. Remarkably, the complexes exhibit low QYs (<10%) in solution but much more intense emission features in the solid state. This phenomenon may be related to aggregation-induced emission enhancement (AIEE), in which the intramolecular rotation of the flexible structural element is limited in the solid state, resulting in higher PL efficiency.

The luminescence decay profiles of zinc complexes were measured at optimal excitation wavelengths. The detailed data are summarized in Table 6. For both solid samples and solutions, the emission decays can only be approximated by monoexponential functions. The general trend is that the luminescence lifetimes in the solid state ($\tau = 5.8\text{--}9.1$ ns) are longer than in solution ($\tau = 3.0\text{--}3.8$ ns), which may be due to their less polar nature in the solid state.

3.6. OLED—Performances

To evaluate and compare the EL properties of **2a–h** complexes, we used them as emitting materials in the fabrication of OLED devices by vacuum deposition. The EL cells were constructed as follows: ITO/PEDOT:PSS/complexes/TPBi/(Ca|Al), in which complexes **2a–h** act as emitters, PEDOT:PSS (poly(3,4-ethylenedioxythiophene) polystyrene sulfonate) is a hole injector, TPBi 1,3,5-tris(*N*-phenylbenzimidazol-2-yl)benzene is an electron transporter, and Ca/Al alloy served as the cathode

For all eight cells obtained, EL was detected at voltages higher than 3.4–4.2 V. The EL was perceived by the eye as blue or blue–green. EL spectra (Figure 9), in general by the shape and position of the maximum coincide with the spectra of PL, which indicates that the complexes act as emitters and emission signals from the electroplex or excimer/exciple in these devices at electroexcitation, are not detected. The applied voltage has no effect on the position of the peak of the emitted light. From Table 7, showing the performance of the OLEDs, it is clear that the best values of performance and brightness are demonstrated by complexes **2c,f,g**. The luminescence intensity of devices is directly proportional to the increase in voltage. Thus, at voltage values of 11–12 V, the brightness reaches more than 1100–6300 cd/m². A further increase in the bias voltage leads to electrical breakdown, leading to rapid cell destruction. Complex **2g**, with a 3,5-difluorophenyl moiety, shows the highest device efficiency, with a current efficiency of 19.7 cd A⁻¹ and an EQE_{max} of 4.8%, which can be attributed to its high PLQY, efficient energy transfer between the layers of the device, and excellent quality of the thin film. It should be noted that the EQE value at 100 Cd more adequately characterizes the OLED performance in practice and is not much lower than the maximum value.

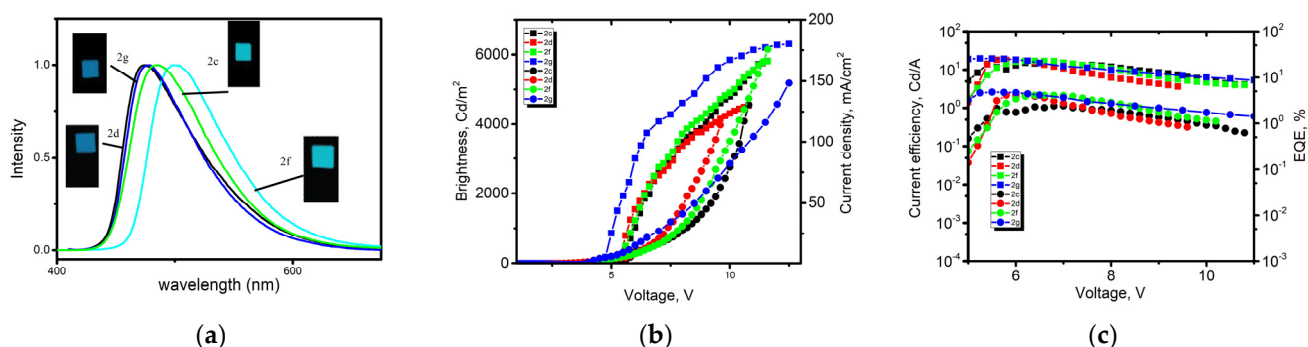


Figure 9. Electroluminescence spectra (a), luminance–voltage–current density characteristics (b) EQE and current efficiency versus current density (c) of devices containing **2c,d,f,g**.

Table 7. Electroluminescence characteristics of nondoped OLEDs.

Device	EL λ_{\max} , nm	Turn-On Voltage, V	Max. Brightness (cd/m ²)	Current Efficiency cd/A	EQE _{max} /EQE _{100Cd} , %
2a	486	4.8	1100	12.6	2.1/1.9
2b	488	4.1	3240	15.0	4.3/3.9
2c	488	4.6	5850	15.4	2.4/2.2
2d	474	4.5	4550	18.0	4.1/3.6
2e	501	4.4	1450	12.2	2.2/2.0
2f	499	4.5	5910	16.9	4.1/3.8
2g	479	4.0	6300	19.7	4.8/4.5
2h	468	4.2	3650	11.1	2.1/1.8

In order to improve the EL parameters, devices containing complex **2g** doped (weight doping concentrations of 5 wt %) with the host matrix with different host molecules (mCP, NPB, TAPC, and CBP) were fabricated and examined. CBP-, NPB-, and TAPC-based devices showed worse performance compared to the underdoped systems due to unfavorable energy transfer from host to guest, as evidenced by the appearance of additional bands in the EL spectrum associated with matrix subwavelength emission. At the same time, the performance using mCP was better, both in terms of brightness and efficiency (Table 8).

Table 8. Electroluminescence characteristics of OLEDs containing **2g** doped to different hosts.

Host Matrix	EL λ_{\max} , nm	Max. Brightness (Cd/m ²)	Current Efficiency Cd/A	EQE _{max} /EQE _{100Cd} , %
mCP	478	8120	21.1	5.1/4.7
NPB	480	3150	11.6	2.2/2.0
TAPC	476, 409	950	6.9	0.9/0.5
CBP	477, 405	1400	7.5	0.95/0.5

3.7. Biological Activity

The obtained azomethines **1a–h** and zinc(II) **2a–h** complexes were tested for their protistocidal, fungistatic, and antibacterial activities. The results of the tests are summarized in Table 9.

Table 9. Protistocidal, fungistatic, and antibacterial activities of azomethines **1a–h** and zinc complexes **2a–h**.

Compound	Protistocidal Activity <i>Colpoda steinii</i> , µg/mL	Fungistatic Activity, Inhibition Zone Diameter, mm <i>Penicillium italicum</i>	Antibacterial Activity, Inhibition Zone Diameter, mm	
			<i>Staphylococcus aureus</i>	<i>Escherichia coli</i>
1a (2-F)	15.6	0	8	10
1b (4-F)	7.8	0	10	8
1c (2,4-F2)	250	0	0	7
1d (2,5-F2)	>500	0	0	10
1e (2,6-F2)	125	0	7	0
1f (3,4-F2)	>500	0	0	8
1g (3,5-F2)	500	0	0	8
1h (2,4,6-F3)	62.5	0	0	0
2a (2-F)	>500	0	8	7
2b (4-F)	125	0	0	0
2c (2,4-F2)	>500	0	0	7
2d (2,5-F2)	>500	0	7	0
2e (2,6-F2)	>500	0	8	7
2f (3,4-F2)	1.9	0	0	8
2g (3,5-F2)	500	0	10	7
2h (2,4,6-F3)	250	0	0	0
Chloroquine (Delaguil).	7.8	-	-	-
Baycox (Toltrazuril)	62.5	-	-	-
Fundazol	-	40	-	-
Furazolidone	-	-	20	18

It was found that neither ligands **1a–h** nor zinc complexes **2a–h** have fungistatic activity against *Penicillium italicum*. Among azomethines, only compounds **1a,b,e** had antibacterial activity against *Staphylococcus aureus*. Their activity was 2–2.5 times weaker than the reference drug furazolidone in the cases of **1a,b** containing one fluorine atom in the amine part, and 2.8 times in the case of **1e** containing two fluorine atoms. Against *Escherichia coli*, **1a–d** and **1f,g** were active. The activity of **1a,d** was 1.8 times weaker than that of furazolidone, the activity of **1b,f,g** was 2.25 times weaker, and that of **1c** was 2.6 times weaker. Azomethines **1c,d,f–h** and **1e,h** did not show antibacterial activity against *Escherichia coli* and against *Staphylococcus aureus*, respectively.

Complexes **2a,d,e,g**, containing one or two fluorine atoms in the amine part of the ligand, showed bacteriostatic activity against *Staphylococcus aureus* that is more than two times lower than furazolidone. The same level of antibacterial activity relative to furazolidone is exhibited by complexes **2a,c,e–g** against *Escherichia coli*. Complexes **2b,c,f,h** were not active against *Staphylococcus aureus* and **2b,d,h** against *Escherichia coli*. The azomethines **1a,c,f,h** and their complexes had almost the same antibacterial activity. While **1b** had moderate bacteriostatic activity, its complex **2b** is inactive. The activity of **1e** and **2e** is almost similar against *Staphylococcus aureus*. Ligands **1d,g** were not active against *Staphylococcus aureus*, while complexes **2d,g** showed medium activity.

In the study of protistocidal properties (Table 9), it was found that azomethines **1a,b**, containing one fluorine atom, had high activity. The activity of **1b** was the same as that of the reference drug chloroquine and eight times stronger than the activity of the second reference drug, toltrazuril, while the activity of **1a** was four times higher than that of toltrazuril but twice as weak as chloroquine. The compound **1h**, containing three fluorine atoms in the amine part of azomethine, showed the same activity as toltrazuril but was eight times weaker than chloroquine. Azomethines **1c,e,g** showed weak protistocidal activity, which was 2–8 times weaker than that of toltrazuril. The compounds **1d,f** did not show protistocidal activity.

Among the complexes **2a–h**, the most active against *Colpoda steinii* is **2f**, which contains fluorine atoms in the three and four positions of the amine part of the ligand, the activity of which is 4.1 times stronger than that of chloroquine and 33 times higher than that of toltrazuril. The activity of **2b,g,h** was weaker than that of toltrazuril by two, eight, or

four times, respectively. The protistocidal activity of **2a–h** decreased compared to **1a–h**, except for **2f**, which contained fluorine atoms in the three and four positions of the amine part of the ligand. The compound **1f** had no protistocidal activity, **2f** exhibited 4.1 times stronger activity than chloroquine and 33 times stronger than toltrazuril. At the same time, complexes **2a,c–e**, containing fluorine atoms in the *ortho*-position of the amine part of the ligand, showed no protistocidal activity.

When comparing the biological activity of chloro- [10,11] and fluoro-substituted *N*-[2-(phenyliminomethyl)phenyl]-4-methylbenzenesulfamides, it was found that azomethine **1b** has antibacterial activity against *Staphylococcus aureus* (50% of the activity of furazolidone), whereas its 4-chloro-substituted analog does not have such activity. Azomethine with 3,4-difluoroaniline **1f** has no activity, while its 3,4-dichlorosubstituted analog has an activity that is 45% of that of furazolidone. Against *Escherichia coli*, 4-fluorosubstituted **1b** and its 4-chlorosubstituted analog showed equal activity, 3,4-difluorosubstituted **1f** had activity amounting to 45% of that of furazolidone, and azomethine with 3,4-dichloroaniline had no activity. In the case of the protistocidal activity in azomethines, the substitution of chlorine in the four positions of the aniline moiety with fluorine leads to a strong increase in activity, which is comparable to that of chloroquine.

Among the zinc complexes of chloro- and fluoro-substituted *N*-[2-(phenyliminomethyl)phenyl]-4-methylbenzenesulfamide, only the 4-chloro-substituted complex was found to have antimicrobial properties against *Staphylococcus aureus* [10], and the 4-fluoro-substituted **2f** was the most active against *Escherichia coli*. In the case of protistocidal activity, the substitution of chlorine atoms in the 4-chloro- and 3,4-dichloro-substituted complexes, which do not possess this activity [10], with fluorine atoms leads to the appearance of strong protistocidal activity. So, 4-fluoro-substituted **2b** has an activity that is 50% of that of toltrazuril, and 3,4-difluoro-substituted **2f** is 4.1 times stronger than chloroquine and 33 times stronger than toltrazuril.

4. Conclusions

The eight new azomethine compounds of *N*-[2-(phenyliminomethyl)phenyl]-4-methylbenzenesulfonamides derivatives with fluorine-substituted anilines and their zinc(II) complexes were obtained. The composition and structure of the obtained compounds were determined by IR, ¹H NMR spectroscopy, and elemental analysis. The structures of two azomethines *N*-[2-[(*E*)-(2,5-difluorophenyl)iminomethyl]phenyl]phenyl]-4-methylbenzenesulfonamide and *N*-[2-[[(*E*)-(3,4-difluorophenyl)iminomethyl]phenyl]phenyl]-4-methylbenzenesulfonamide and their zinc(II) complexes, as well as Bis[*N*-(*p*-tolylsulfonyl)-2-[(*E*)-(2,4,6-trifluorophenyl)iminomethyl]anilino]zinc(II) were determined by single-crystal X-ray diffraction. Azomethines in the solid state have PL-band maxima in the region λ_{PI} 567–589 nm, with PL quantum yields from 10.3 to 43.9%, which are 4–16 times higher than the corresponding quantum yields for unsubstituted azomethines. In the PL spectra of zinc(II) complexes, the maxima of the PL bands undergo a hypsochromic shift to 476–506 nm compared to free ligands, and their quantum yields range from 22.3 to 42.2%. The obtained quantum yields for zinc complexes with fluorine-substituted ligands are 2–4 times higher compared to the quantum yield for the zinc complex with unsubstituted ligands. OLEDs were made using zinc complexes as emissive layers, for which the maximum brightness was from 950 to 8120 cd/m² with a current efficiency of 6.9 to 21.1 cd/A. Obtained results are comparable and even higher in some cases with the same class of luminophores [28–32]. The obtained azomethines and zinc(II) complexes were tested for their protistocidal, fungistatic, and antibacterial activities. It was shown that the replacement of chlorine atoms in 3,4-dihalophenyl-substituted complexes with fluorine atoms leads to the appearance of strong protistocidal activity in the complexes.

Supplementary Materials: The following supporting information can be downloaded at: <https://www.mdpi.com/article/10.3390/ma17020438/s1>, Table S1. Selected crystallographic data for compounds **1d** and **1f**. Table S2. Selected crystallographic data for compounds **2d**, **2h** and **2f**.

Author Contributions: A.S.B.—conceptualization, investigation, writing—original draft preparation; V.G.V.—visualization, investigation, writing—original draft preparation; M.S.M.—investigation; Y.V.K.—conceptualization; V.A.L.—data curation; A.L.T.—data curation; A.A.K.—writing—review and editing; A.A.Z.—investigation; E.V.B.—investigation, data curation; A.N.G.—data curation, conceptualization; W.L.—writing—review and editing. All authors have read and agreed to the published version of the manuscript.

Funding: The research was carried out with the financial support of the Ministry of Science and Higher Education of the Russian Federation (State assignment in the field of scientific activity 2023, FENW-2023-0011) and the federal program Prioritet-2030 (Crimean Federal University V.I. Vernadsky).

Institutional Review Board Statement: Not applicable.

Informed Consent Statement: Not applicable.

Data Availability Statement: The data presented in this article are openly available.

Acknowledgments: IR and ¹H NMR spectra were obtained using facilities of the “Molecular Spectroscopy” Multiuser Center of Southern Federal University. The authors would like to acknowledge Alexander Klimenko (North-Caucasian Zonal Scientific Research Veterinary Institute—Branch of the Federal State Budget Scientific Institution “Federal Rostov Agricultural Research Centre”) for organizing the biological tests and the resulting interpretations.

Conflicts of Interest: The authors declare no conflicts of interest.

References

1. Pushkarev, A.P.; Bochkarev, M.N. Organic electroluminescent materials and devices emitting in the UV and NIR regions. *Russ. Chem. Rev.* **2016**, *85*, 1338. [\[CrossRef\]](#)
2. Kozlov, M.I.; Aslandukov, A.N.; Vashchenko, A.A.; Medvedko, A.V.; Aleksandrov, A.E.; Grzibovskis, R.; Goloveshkin, A.S.; Lepnev, L.S.; Tameev, A.R.; Vembris, A.; et al. On the development of a new approach to the design of lanthanide-based materials for solution-processed OLEDs. *Dalton Trans.* **2019**, *48*, 17298–17309. [\[CrossRef\]](#) [\[PubMed\]](#)
3. Nehra, K.; Dalal, A.; Hooda, A.; Bhagwan, S.; Saini, R.K.; Mari, B.; Kumar, S.; Singh, D. Lanthanides β-diketonate complexes as energy-efficient emissive materials: A review. *J. Mol. Struct.* **2022**, *1249*, 131531. [\[CrossRef\]](#)
4. Tan, R.H.C.; Motevalli, M.; Abrahams, I.; Wyatt, P.B.; Gillin, W.P. Quenching of IR Luminescence of Erbium, Neodymium, and Ytterbium β-Diketonate Complexes by Ligand C–H and C–D Bonds. *J. Phys. Chem. B* **2006**, *110*, 24476–24479. [\[CrossRef\]](#) [\[PubMed\]](#)
5. Hyre, A.S.; Doerrer, L.H. A structural and spectroscopic overview of molecular lanthanide complexes with fluorinated O-donor ligands. *Coord. Chem. Rev.* **2020**, *404*, 213098. [\[CrossRef\]](#)
6. Winkless, L.; Tan, R.H.C.; Zheng, Y.; Motevalli, M.; Wyatt, P.B.; Gillin, W.P. Quenching of Er(III) luminescence by ligand C–H vibrations: Implications for the use of erbium complexes in telecommunications. *Appl. Phys. Lett.* **2006**, *89*, 111115. [\[CrossRef\]](#)
7. Hasegawa, Y.; Wada, Y.; Yanagida, S. Strategies for the design of luminescent lanthanide(III) complexes and their photonic applications. *J. Photochem. Photobiol. C Photochem. Rev.* **2004**, *5*, 183–202. [\[CrossRef\]](#)
8. Artizzu, F.; Mercuri, M.L.; Serpe, A.; Deplano, P. NIR-emissive erbium–quinolinolate complexes. *Coord. Chem. Rev.* **2011**, *255*, 2514–2529. [\[CrossRef\]](#)
9. Zheng, Y.; Motevalli, M.; Tan, R.H.C.; Abrahams, I.; Gillin, W.P.; Wyatt, P.B. Near IR luminescent rare earth 3,4,5,6-tetrafluoro-2-nitrophenoxide complexes: Synthesis, X-ray crystallography and spectroscopy. *Polyhedron* **2008**, *27*, 1503–1510. [\[CrossRef\]](#)
10. Burlov, A.S.; Vlasenko, V.G.; Milutka, M.S.; Koshchienko, Y.V.; Makarova, N.I.; Lazarenko, V.A.; Trigub, A.L.; Kolodina, A.A.; Zubenko, A.A.; Metelitsa, A.V.; et al. Synthesis, structure, spectral-luminescent properties and biological activity of chlorine-substituted N-[2-(phenyliminomethyl)phenyl]-4-methylbenzenesulfamide and their zinc(II) complexes. *Int. J. Mol. Sci.* **2022**, *23*, 15259. [\[CrossRef\]](#)
11. Milutka, M.S.; Burlov, A.S.; Vlasenko, V.G.; Koshchienko, Y.V.; Makarova, N.I.; Metelitsa, A.V.; Korshunova, E.V.; Trigub, A.L.; Zubenko, A.A.; Klimenko, A.I. Synthesis, Structure, Spectral-Luminescent Properties, and Biological Activity of Chlorine-Substituted Azomethines and Their Zinc(II) Complexes. *Russ. J. Gen. Chem.* **2021**, *91*, 1706–1716. [\[CrossRef\]](#)
12. Chernyshov, A.A.; Veligzhanin, A.A.; Zubavichus, Y.V. Structural Materials Science End-Station at the Kurchatov Synchrotron Radiation Source: Recent Instrumentation Upgrades and Experimental Results. *Nucl. Instrum. Methods Phys. Res. Sect. A* **2009**, *603*, 95–98. [\[CrossRef\]](#)
13. Newville, M. EXAFS analysis using FEFF and FEFFIT. *J. Synchrotron Radiat.* **2001**, *8*, 96–100. [\[CrossRef\]](#) [\[PubMed\]](#)
14. Zabinski, S.I.; Rehr, J.J.; Ankudinov, A.; Alber, R.C. Multiple-scattering calculations of x-ray-absorption spectra. *Phys. Rev.* **1995**, *52*, 2995–3009. [\[CrossRef\]](#)
15. Svetogorov, R.D.; Dorovatovskii, P.V.; Lazarenko, V.A. Belok/XSA diffraction beamline for studying crystalline samples at Kurchatov Synchrotron Radiation Source. *Cryst. Res. Technol.* **2020**, *55*, 1900184. [\[CrossRef\]](#)

16. Kabsch, W. XDS. *Acta Crystallogr. Sect. D Biol. Crystallogr.* **2010**, *66*, 125–132. [[CrossRef](#)]
17. Sheldrick, G.M. SHELXT—Integrated space-group and crystal-structure determination. *Acta Crystallogr. Sect. A Found. Adv.* **2015**, *71*, 3–8. [[CrossRef](#)]
18. Dolomanov, O.V.; Bourhis, L.J.; Gildea, R.J.; Howard, J.A.; Puschmann, H. OLEX2: A complete structure solution, refinement and analysis program. *J. Appl. Crystallogr.* **2009**, *42*, 339–341. [[CrossRef](#)]
19. Sheldrick, G.M. Crystal structure refinement with SHELXL. *Acta Crystallogr. Sect. C Struct. Chem.* **2015**, *71*, 3–8. [[CrossRef](#)]
20. Burlov, A.S.; Vlasenko, V.G.; Koshchienko, Y.V.; Makarova, N.I.; Zubenko, A.A.; Drobin, Y.D.; Fetisov, L.N.; Kolodina, A.A.; Zubavichus, Y.V.; Trigub, A.L.; et al. Synthesis, characterization, luminescent properties and biological activities of zinc complexes with bidentate azomethine Schiff-base ligands. *Polyhedron* **2018**, *154*, 65–76. [[CrossRef](#)]
21. Burlov, A.S.; Vlasenko, V.G.; Koshchienko, Y.V.; Makarova, N.I.; Zubenko, A.A.; Drobin, Y.D.; Borodkin, G.S.; Metelitsa, A.V.; Zubavichus, Y.V.; Garnovskii, D.A. Complexes of zinc(II) with N-[2-(hydroxyalkyliminomethyl)phenyl]-4-methylbenzenesulfonamides: Synthesis, structure, photoluminescence properties and biological activity. *Polyhedron* **2018**, *144*, 249–258. [[CrossRef](#)]
22. Chernova, N.I.; Ryabokobylko, Y.S.; Brudz', V.G.; Bolotin, B.M. 2-Tosylaminobenzaldehyde and its substitutes. *Zh. Org. Khim.* **1971**, *7*, 1680–1687.
23. Obodovskaya, A.E.; Starikova, Z.A.; Trunov, V.K.; Bolotin, B.M. Crystal and molecular structure of N-(2-tosylaminobenzylidene)aniline. *J. Struct. Chem.* **1981**, *22*, 78–81. [[CrossRef](#)]
24. Obodovskaya, A.E.; Starikova, Z.A.; Trunov, V.K.; Bolotin, B.M. Intramolecular hydrogen bonds and the crystal structure of N-(2-tosylaminobenzylidene)benzylamine. *J. Struct. Chem.* **1981**, *22*, 82–85. [[CrossRef](#)]
25. Desiraju, G.R. (Ed.) *Crystal Design: Structure and Function. Perspectives in Supramolecular Chemistry*; Wiley-VCH: Chichester, UK, 2002.
26. Castro, J.; Cabaleiro, S.; Perez-Lourido, P.; Romero, J.; Garcia-Vazquez, J.A.; Sousa, A. Electrochemical Synthesis and Characterization of Zinc(II) Complexes with [(4-Methylphenyl)Sulfonyl]-1H-Amido-2-Phenyl-2-Oxazolines. *Z. Anorg. Allg. Chem.* **2002**, *628*, 1210–1217. [[CrossRef](#)]
27. Yang, L.; Powell, D.R.; Houser, R.P. Structural variation in copper(I) complexes with pyridylmethylamide ligands: Structural analysis with a new four-coordinate geometry index, τ_4 . *Dalton Trans.* **2007**, *9*, 955–964. [[CrossRef](#)] [[PubMed](#)]
28. Dumur, F. Zinc complexes in OLEDs: An overview. *Synth. Met.* **2014**, *195*, 241–251. [[CrossRef](#)]
29. Bizzarri, C.; Spuling, E.; Knoll, D.M.; Volz, D.; Brase, S. Sustainable metal complexes for organic light-emitting diodes (OLEDs). *Coord. Chem. Rev.* **2018**, *373*, 49–82. [[CrossRef](#)]
30. Singh, D.; Nishal, V.; Bhagwan, S.; Saini, R.K.; Singh, I. Electroluminescent materials: Metal complexes of 8-hydroxyquinoline—A review. *Mater. Des.* **2018**, *156*, 215–228. [[CrossRef](#)]
31. Rashamuse, T.J.; Mohlala, R.L.; Coyanis, E.M.; Magwa, N.P. A Review: Blue Fluorescent Zinc (II) Complexes for OLEDs—A Last Five-Year Recap. *Molecules* **2023**, *28*, 5272. [[CrossRef](#)]
32. Diana, R.; Panunzi, B.; Tuzi, A.; Caruso, U.J. Two tridentate pyridinyl-hydrazone zinc (II) complexes as fluorophores for blue emitting layers. *Mol. Struct.* **2019**, *1197*, 672–680. [[CrossRef](#)]

Disclaimer/Publisher's Note: The statements, opinions and data contained in all publications are solely those of the individual author(s) and contributor(s) and not of MDPI and/or the editor(s). MDPI and/or the editor(s) disclaim responsibility for any injury to people or property resulting from any ideas, methods, instructions or products referred to in the content.